Filament transport, warm ions and erosion in ASDEX Upgrade L-modes

G. Birkenmeier,[1,2,*] P. Manz,[1,2] D. Carralero,[1] F. M. Laggner,[3] G. Fuchert,[1] K. Krieger,[1] H. Maier,[1] F. Reimold,[1] K. Schmid,[1] R. Dux,[1] T. Pütterich,[1] M. Willensdorfer,[1] E. Wolfrum,[1] and the ASDEX Upgrade Team

[1] *Max Planck Institute for Plasma Physics, Boltzmannstr. 2, 85748 Garching, Germany*
[2] *Physik-Department E28, Technische Universität München, 85748 Garching, Germany*
[3] *Institute of Applied Physics, Vienna University of Technology, Fusion@ÖAW, Wiedner Hauptstr. 8-10, 1040 Vienna, Austria*

The dynamics of blob filaments are investigated in the scrape-off layer of ASDEX Upgrade by means of lithium beam emission spectroscopy. A comparison of the measurements in L-mode with a recently developed analytical blob model based on a drift-interchange-Alfvén fluid model indicates an influence of a finite ion temperature on the blob dynamics which has typically been neglected in other blob models. The blob dynamics agree well with the sheath-connected regime at lower plasma densities, and inertial effects play only a minor role. At higher densities, a transition into another regime with large blob amplitudes and increased transport is found. This points to a prominent role of blob transport at higher Greenwald fractions. On the basis of the measured blob properties, the erosion on plasma facing components is estimated. For pure deuterium plasmas, the high ion temperatures of blobs lead to a dominant erosion induced by blobs. However, if an impurity concentration of 1% is taken into account, the blob-induced erosion plays a minor role and background plasma parameters determine the total gross erosion.

PACS numbers: 52.25.Xz, 52.25.Fi, 52.35.Ra, 52.55.Fa

I. INTRODUCTION

For a safe and economic operation of a tokamak fusion power plant, the erosion of the first wall must be kept as low as possible in order to avoid expensive material replacements and influx of impurities into the plasma. While divertor tiles in a future fusion reactor are envisaged to be tungsten monoblocks, the main chamber can only be coated with a thin layer of low-erosion material in order to be compatible with the neutronics requirements for tritium breeding concepts [1]. Since a significant fraction of the total power deposition [2, 3] and large erosion levels [4] can occur at the main chamber wall of existing devices, estimations of wall degradation and extrapolation to future devices is needed.

The transport processes in the scrape-off layer (SOL) determine the local plasma temperature and density in front of the plasma facing components (PFCs) and therefore set the heat flux and erosion rate at the wall. While the temporally averaged electron temperature T_e in the SOL is comparatively low, the ion temperature T_i is typically much higher due to the lower parallel heat conductivity of ions. Measurements with a retarding field analyzer (RFA) [5] have shown, that the ion temperatures T_i are even higher in outward convected density filaments, so called blobs [6, 7]. These higher ion temperatures and peak densities δn of the blobs could therefore contribute significantly to the erosion of the first wall due to the strong temperature dependence of the sputtering yield [8]. For a reliable prediction of the influence of these filaments on SOL transport and erosion rates at the first wall in future fusion devices, a physical understanding of their generation and propagation is needed. This paper focuses on the impact of warm ions on the dynamics of blob filaments and describes an estimation of erosion rates based on measurements with the lithium beam emission spectroscopy (Li-BES) diagnostic and an RFA in the SOL of ASDEX Upgrade.

II. BLOB MEASUREMENTS WITH LI-BES

By means of lithium beam emission spectroscopy [9] the dynamics of blobs in the SOL of ASDEX Upgrade is investigated. The Li-BES diagnostic measures the Li_{2p-2s} line emission of a beam of neutral lithium atoms colliding with plasma particles. The emission is proportional to the electron density in the far SOL [10]. Further inside the plasma, this relation is not valid anymore, and collisional-radiative modelling is required in order to reconstruct the electron density profile in the edge [11]. At ASDEX Upgrade, a 45 keV neutral lithium beam is injected from the low-field side 32 cm above the outboard midplane. For the blob studies we use a horizontal array of 26 lines of sight (LOS) which detect the Li_{2p-2s} line emission by means of optical filters and photomultipliers. The LOS have a radial distance of 6 mm and the observation volume of a single LOS is an ellipse with a width of 5 mm and a height of 12 mm. Details of the Li-BES setup and the relation of the line emission intensity response to a density blob are described in Ref. [10].

The Li-BES raw data, i.e. the Li_{2p-2s} line emission detected with the 15 outermost LOS, is analyzed by a conditional averaging technique in order to detect blobs.

*Electronic address: gregor.birkenmeier@ipp.mpg.de

Details of this technique are described in Ref. [12]. Whenever the raw signal of a Li-BES channel at a chosen radial reference position in the far SOL exceeds the threshold of 2.5σ (σ is the standard deviation), the event is treated as a blob. By means of the conditonal averaging technique, the amplitude δn, the radial size a, the radial velocity v_r, the self-correlation time τ_{blob}, and the frequency of the blobs in different plasma regimes is determined. In low density L-mode discharges, the radial size of the blobs is a few centimeters and it depends only weakly on the magnetic field strength [12]. Maximum velocities v_r of about 1 km/s and blob peak amplitudes of $\delta n \approx 6 \cdot 10^{18}\,\mathrm{m}^{-3}$ are found. The relative amplitudes of blobs $\delta n/n$ are therefore of the order of unity. The self-correlation time or residence time τ_{blob}, which corresponds to the time span during that the blob passes the reference channel, amounts to 50 to 150 μs and increases with the parallel connection length $L_{||}$.

A. Blob Scaling in Low Density L-Modes

The measurement results from a set of low density L-modes (see Ref. [12] for discharge details) are compared to analytical blob scaling laws. According to blob scaling laws derived from a drift-Alfvén fluid model for warm ions [13], the most stable size of the blob is given by

$$a^* = \sqrt[5]{8(1+\tau_i)}\rho_s^{4/5} L_{||}^{2/5}/R^{1/5} \qquad (1)$$

with the ratio of ion to electron temperature $\tau_i = T_i/T_e$, drift parameter $\rho_s = \sqrt{T_e m_i}/eB$, the ion mass m_i, magnetic field strength B, parallel connection length $L_{||}$ and major plasma radius R. The corresponding *warm ion sheath-connected* velocity scaling is

$$\frac{v_r}{c_s} = (1+\tau_i)\left(\frac{\rho_s}{a}\right)^2 \frac{L_{||}}{R}\frac{\delta n}{n} \qquad (2)$$

with sound velocity $c_s = \sqrt{(T_e+T_i)/m_i}$. Fig. 1a shows the relation of the measured blob size a to the scaling law a^* according to Eq. 1 at the radial position of $\rho_{\mathrm{pol}} = 1.044$ (ρ_{pol} is the normalized poloidal flux coordinate). Here, we assume that the measured *radial* blob size is equal to its *poloidal* extent in order to relate it to the scaling law which was derived for the poloidal blob size a^*. Each data point in Fig. 1 corresponds to an evaluation of a time interval of 400 ms from different discharges. The error bars are the statistical variations (standard deviation) determined in several subseries with a length of 56 ms each (except for the horizontal error bars in (a) which correspond to the propagation of uncertainty according to Eq. 1). The warm ion scaling (diamonds) for $\tau_i = 3$ predicts blob sizes a^* in the range of 1 cm, and therefore fits better to the measured values a than the cold ion scaling with $\tau_i = 0$ and blob sizes in the range of $a^* \approx 0.5$ cm (triangles). This indicates that warm ion effects play a role in blob dynamics.

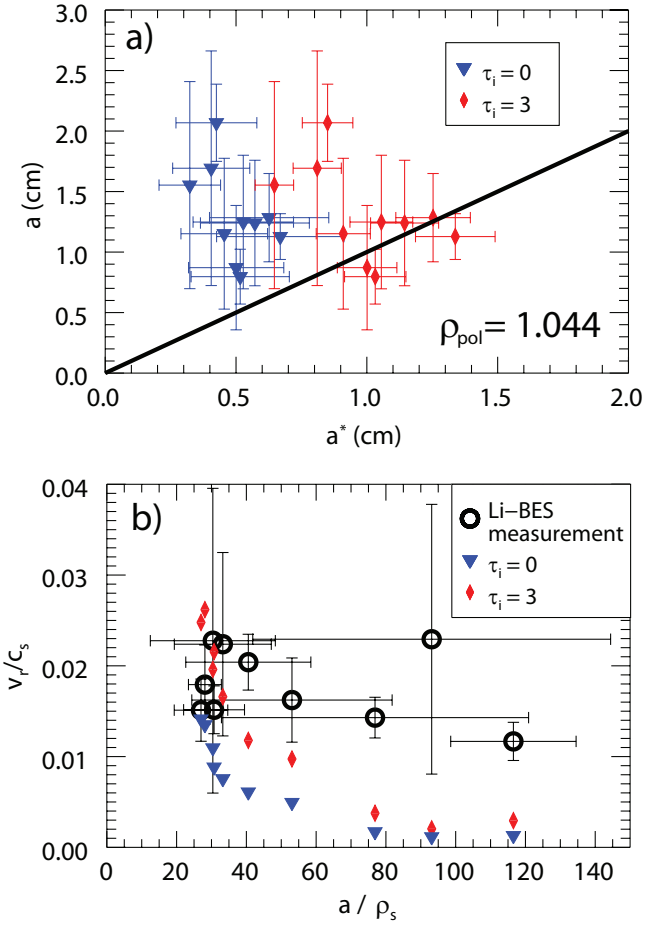

FIG. 1: (a) The blob size a^* (Eq. 1) from the scaling law for cold ions (triangles) underestimates the measured blob size a. The agreement is better for the warm ion scaling (diamonds). The black line corresponds to perfect agreement between measurement and theory. (b) Likewise, the normalized velocities for the warm ion scaling (diamonds) fit better to the measurements (circles) than the cold ion scaling (triangles). Adapted from [12].

The measured velocities v_r (circles) are normalized to the local values of the sound velocity c_s and plotted against the measured normalized blob sizes a/ρ_s in Fig. 1b. While an inertial scaling overpredicts the absolute values of the measured velocities by an order of magnitude (not shown), the sheath-connected scaling law for cold ions according to Eq. 2 with $\tau_i = 0$ (triangles) is at least for the smaller blobs in the same range as the measured velocities. For warm ions the agreement between measurement and scaling law ($\tau_i = 3$) is somewhat better (diamonds). Both scalings share a decreasing tendency with increasing blob size as it is expected for sheath-connected blobs. This tendency is not that obvious for the measured values. In summary, the measured blob sizes and velocities in low density L-modes agree best with scaling laws for sheath-connected blobs. The improved agreement for warm ions indicate that warm ion effects play a role in the blob dynamics. The measure-

ments fit best to the scaling laws for $\tau_i = T_i/T_e = 3$, which is supported by direct measurements of ion temperatures in the SOL of ASDEX Upgrade with an RFA [5].

B. Blob Properties at Higher Density

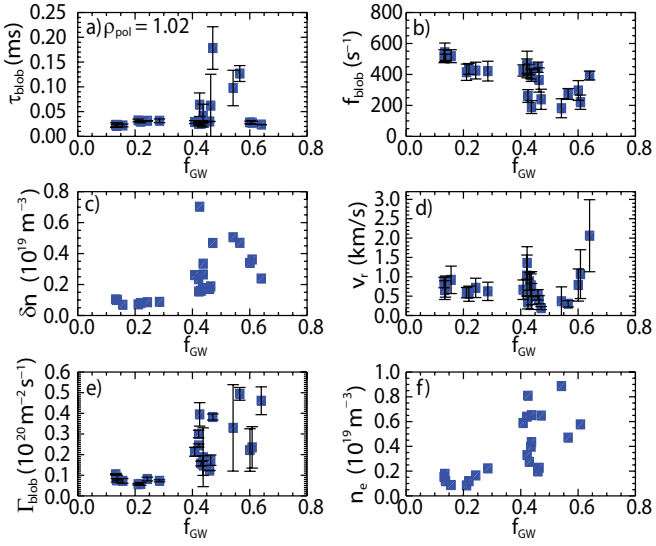

FIG. 2: With rising density (expressed as Greenwald fraction $f_{GW} = n/n_{GW}$), the blobs transition from a sheath-connected regime into a regime of enhanced convective transport associated with larger residence time (a), lower blob frequency (b), larger amplitude (c), higher velocity (d), and increased blob transport (e). The local background density at ρ_{pol}=1.02 (f) is likewise increased.

At higher densities, the convective blob transport increases significantly above a critical core density threshold corresponding to a Greenwald fraction of $f_{GW} = n/n_{GW} \approx 0.45$ measured in another set of L-mode discharges with a plasma current of 0.8 MA. This transition into a regime of increased blob transport is found to be related to divertor detachment, and it was shown that higher resistivity along the magnetic field line can increase the blob transport significantly [14]. The change in different parameters depending on Greenwald fraction f_{GW} is shown in Fig. 2 for $\rho_{\rm pol} = 1.02$. In comparison to the low density regime ($f_{GW} < 0.45$), the blob amplitudes δn (Fig. 2c) rise up to the fivefold in the high density regime ($f_{GW} > 0.45$), the blob residence time $\tau_{\rm blob}$ (Fig. 2a) increases by a factor of three, the velocities v_r double (Fig. 2d), and the number of 2.5σ-blobs per second $f_{\rm blob}$ goes down (Fig. 2b). Similar observations are reported in [15]. In this regime, the blob transport $\Gamma_{\rm blob} = \tau_{\rm blob} f_{\rm blob} \delta n v_r$ perpendicular to the magnetic field increases by one order of magnitude from minimum $\Gamma_{\rm blob} \approx 0.5 \cdot 10^{19}\,{\rm m^{-2}s^{-1}}$ in the low density regime to maximum $\Gamma_{\rm blob} \approx 5.0 \cdot 10^{19}\,{\rm m^{-2}s^{-1}}$ at higher densities. Due to this enhanced perpendicular transport, a flat shoulder in the density profile is formed [14] leading to local densities $n(\rho_{\rm pol} = 1.02)$ of up to $1 \cdot 10^{19}\,{\rm m^{-3}}$ (Fig. 2f) in the far SOL at the outboard midplane.

III. ESTIMATION OF EROSION

By means of the measured blob quantities, we can now estimate the blob induced erosion at PFCs connected with the blobs, and compare it with the erosion as calculated from background profile parameters only. A plasma with a given density n_p, without blobs and without impurities causes a gross erosion, i.e. erosion without redeposition or other secondary effects (e.g. self-sputtering), at the PFC of [16]

$$E_{\rm back} = \frac{1}{2} c_s n_p Y \Delta t \cos\alpha / n_{PFC}. \qquad (3)$$

$E_{\rm back}$ is given in units of length and represents the thickness of eroded PFC material of density n_{PFC} which is exposed to the background plasma for a time span of Δt. Y is the effective sputtering yield (=number of expelled PFC atoms per incident plasma ion) and a non-linear function of T_i and T_e. α is the angle between the velocity vector of the incident ion and the surface normal vector of the PFC at the impact position. For D^+ and C^{4+} it was shown that the impact angle must be chosen as $\alpha \approx 60^o$ [17].

The effective sputtering yield of a tungsten surface in contact with a pure deuterium plasma is shown in Fig. 3a (dashed line). For this calculation, the ions are assumed to be Maxwellian distributed having an energy of [16]

$$E_i = 2k_B T_i - ZeV_s. \qquad (4)$$

The first term is the approximate thermal energy of the ions at the sheath edge and the second term represents the energy of an ion with charge state Z gained in the sheath potential drop V_s. The latter is typically negative for floating conditions and given in units of $k_B T_e$ by

$$\frac{eV_s}{k_B T_e} = 0.5 \ln\left[\left(2\pi\frac{m_e}{m_i}\right)\left(1+\frac{T_i}{T_e}\right)(1-\delta_{se})^{-2}\right] \qquad (5)$$

with electron mass m_e and secondary electron coefficient δ_{se}. We set $\delta_{se} = 0$ (see discussion below) and, in agreement with measurements in the SOL of ASDEX Upgrade at a Greenwald fraction of $f_{GW} = 0.44$ [5], the ion temperature is assumed to be three times higher than the electron temperature ($\tau_i = 3$) resulting in an effective sheath potential drop of $V_s \approx 2.5 k_B T_e/e$. The sputtering yield for a pure deuterium plasma ($Z = 1$) strongly rises above $T_i > 30\,{\rm eV}$, but is negligible below (see Fig. 3a, dashed line).

For the estimation of the erosion of blobs, we consider the following situation. From the measurements we know

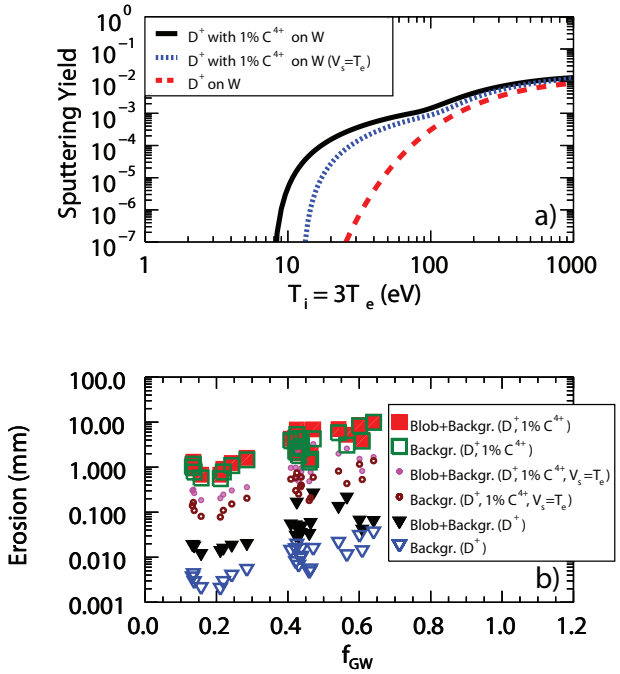

FIG. 3: (a) Effective sputtering yield Y of a tungsten surface in contact with a deuterium plasma without impurities (dashed line), with 1% of C^{4+} impurity concentration (solid line), and with impurities but reduced sheath potential drop (dotted line) for different ion temperatures $T_i = 3 \cdot T_e$. (b) Gross erosion (i.e. erosion without redeposition) at the contact region for one burn year (365 d, 24 h/d) for ASDEX Upgrade L-mode conditions (logarithmic scale) for different impurity concentrations and sheath potentials.

that a blob of density δn stays for the time span of the residence time τ_{blob} within our Li-BES observation volume of a single LOS (purple region in Fig. 4). Since the blob is connected parallel to the magnetic field with a PFC, it passes during the same time span the contact region (orange) on the PFC close to the divertor. A single blob therefore induces an erosion of

$$E_{\mathrm{blob}} = \frac{1}{2} c_{\mathrm{s,blob}} \delta n Y_{\mathrm{blob}} \tau_{\mathrm{blob}} \cos\alpha / n_{PFC}. \qquad (6)$$

A. Erosion of a Pure Deuterium Plasma

For the background plasma (pure deuterium) we now assume $T_i = 18\,\mathrm{eV}$ and $T_e = 7\,\mathrm{eV}$, and for the blobs $T_{\mathrm{i,blob}} = 100\,\mathrm{eV}$ and $T_{\mathrm{e,blob}} = 30\,\mathrm{eV}$ as it was measured with an RFA in comparable discharges at fixed $f_{GW} = 0.44$ [5]. Furthermore, we assume $\Delta t = 31.5 \cdot 10^6\,\mathrm{s}$ corresponding to a full year of plasma operation (burn year) in order to relate our results to the operating conditions in a fusion power plant in terms of pulse duration. For the blobs, we have to multiply Δt by a weighting factor of $w = \tau_{\mathrm{blob}} f_{\mathrm{blob}}$ due to the fact that the blobs exist only for a short fraction of time (typically $w \approx 2$ % of a time trace consist of 2.5σ-blobs). For tungsten we set $n_{PFC} = 6.3 \cdot 10^{28}\,\mathrm{m}^{-3}$, and all other parameters are used as measured and shown in Fig. 2. The result of this estimation according to Eqs. 3 and 6 for different densities of a pure deuterium plasma is shown in Fig. 3b. The erosion E_{back} induced by the background plasma only (open triangles) is typically one order of magnitude smaller than the total erosion $E_{\mathrm{tot}} = E_{\mathrm{blob}} + E_{\mathrm{back}}$ (filled triangles) which accounts for both blob and background induced erosion. This is a striking result since the blobs are only a fraction of time ($w \sim 1/50$ of a second) in contact with the PFC while the background plasma continuously sputters the contact region. But the higher plasma density δn and the substantially higher ion temperature T_i in combination with the non-linear dependence of Y on T_i overcompensate the shorter contact time.

With increasing density both the background induced erosion E_{back} and the total erosion E_{tot} including blobs increase due to the density dependence of Eqs. 3 and 6. While the absolute values of the erosion of the background plasma of maximum $E_{\mathrm{back}} \approx 0.04\,\mathrm{mm}$ is harmless, the total erosion achieves values up to $E_{\mathrm{tot}} \approx 0.4\,\mathrm{mm}$ which could be a concern for the first wall material in future reactor designs.

B. Erosion with 1% Impurity Concentration

As has been shown in previous investigations of sputtering of tungsten PFCs in ASDEX Upgrade [8, 18, 19], even low fractions of impurity concentrations can substantially increase the sputtering yield due to the higher ion mass and charge state Z of impurity ions (compare also Eq. 4). The measured erosion levels could only be explained by erosion models which take into account a few percent of C^{4+} as a placeholder for all low-Z impurities typically present in ASDEX Upgrade. As shown in Fig. 3a (solid line), the effective sputtering yield of a deuterium plasma containing 1% of C^{4+} impurity ions is between 8 eV and 80 eV several orders of magnitude greater than a pure deuterium plasma and significant sputtering sets in already at comparatively low temperatures.

If this effect is now taken into account for the comparison of background and blob induced erosion, the relevance of the higher ion temperatures in blobs decreases. The total erosion including blobs (Fig. 3b, filled squares) is maximum 37% higher than the background erosion only (open squares). Due to the higher charge number $Z = 4$ for impurity ions, the sheath acceleration gains in importance. Therefore, the high ion temperatures in blobs play only a minor role for the effective sputtering yield. Due to the same effect, the sputtering curve is flatter at lower temperatures resulting in small differences of the sputtering yields for background and blob plasma parameters. This is in contrast to the pure deuterium case, where the differences between background and blob sputtering yields could even balance the less

frequent occurence of blobs.

C. Erosion with 1% Impurity Concentration and Reduced Sheath Potential

So far, we used the approximation $V_s \approx 2.5 k_B T_e/e$ assuming $\delta_{se} = 0$ in Eq. 5 for the calculation of the sputtering yields. For finite secondary electron emission $\delta_{se} \neq 0$, however, the sheath potential can be reduced significantly as indicated by measurements in different tokamaks [20–22]. This reduction of the sheath potential decreases the acceleration of the ions in the sheath and therefore reduces the impact of the impurities for the erosion process (see Fig. 3a, dotted line). In order to account for this effect, we determined the erosion for background plasma parameters (open circles) and the total erosion including blobs (filled circles) as an example assuming $V_s = 1 k_B T_e/e$ corresponding to $\delta_{se} = 0.775$ as shown in Fig. 3b. In this case, the absolute erosion levels are reduced by an order of magnitude relative to the case with impurities and $V_s \approx 2.5 k_B T_e/e$, but still much higher than the erosion levels without impurities at all. For finite δ_{se}, the erosion levels with blobs are a factor of two larger than the background erosion only. This reveals again the complementarity of the sheath effect and the influence of blobs on erosion: weak impact of the sheath acceleration involves strong blob contribution and vice versa.

We have to state clearly that Eqs. 3 and 6 are only rough estimates for the evaluation of *gross* erosion. It does not account for redeposition or for the fact that there could exist parallel density and temperature gradients along the magnetic field line. Furthermore, we assumed the same temperatures and temperature ratio $\tau_i = 3$ for the whole density range. However, as it was shown in Ref. [23], τ_i depends on the density and can range from 2 to 8 changing the erosion due to the sheath potential (see Eq. 5). The very high erosion of up to 10 mm in the case with impurity ions at high Greenwald fraction (Fig. 3b, filled squares) is, therefore, an upper limit of a worst case scenario.

On the other hand, the estimations are done for L-mode parameters. In H-mode plasmas, however, significantly higher densities in filaments of edge localized modes (ELMs) [24] (even in scenarios with small ELMs [25]), and hence higher erosion could be achieved. This is possibly of relevance for ITER which will operate in H-mode and at much higher temperatures [26]. Together with the fact that sputtering of Beryllium sets in already at much lower ion temperatures than it is the case for tungsten, this is unfavourable for the first wall in ITER. Another issue, which has not been taken into account in our estimation, is self-sputtering of tungsten which also can increase erosion. Averaged over a whole campaign (6300 s of plasma operation) at ASDEX Upgrade, a net erosion of maximum 100 nm corresponding to a net erosion rate of $1.59 \cdot 10^{-11}$ m/s was measured by means of Rutherford backscattering on baffle tiles [4]. This is only one order of magnitude lower than the gross erosion rate of about $3.17 \cdot 10^{-10}$ m/s (~ 10 mm in one burn year) as derived from our blob erosion model including impurities described above. In this sense, our estimation is not far from reality.

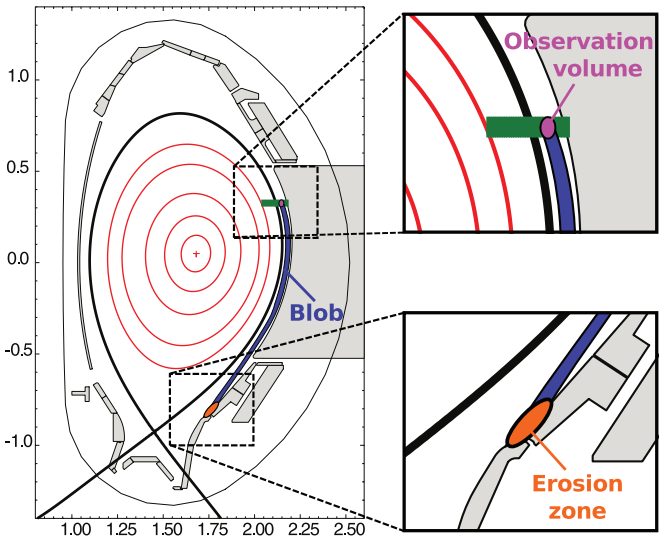

FIG. 4: Schematic of blob induced erosion: A blob (blue) in the SOL passes the observation volume (purple) of the Li-BES diagnostic during a residence time of τ_{blob}. For the same time span τ_{blob}, the blob is connected along the field line to a contact region (orange) on a PFC close to the divertor. The plasma parameters of the blob determine the erosion properties in the contact region.

IV. SUMMARY

We have shown that the blob dynamics measured with Li-BES in low density L-mode discharges at ASDEX Upgrade can be described with simple scaling laws for size and velocities of blobs in the sheath-connected regime. Due to the better agreement of the measured parameters with warm ion scaling laws we conclude that the warm ions play a role in the blob dynamics.

With increasing density the blob properties change. The blobs are getting larger (amplitude and size), faster and stay for a longer period in front of our observation volumes. This regime of increased blob transport is related to an increased resistivity in the SOL parallel to the magnetic field line as shown in Ref. [14].

From the measured blob quantities we estimated the gross erosion for background and blob parameters for a density range from $f_{GW} = 0.1$ to 0.7. The total erosion increases with density. For a pure deuterium plasma, we found that the blobs significantly contribute to the total erosion and exceed the erosion levels of the background profiles by an order of magnitude despite the fact

that the blobs exist only for a short period of time. The higher density and ion temperatures overcompensate the short life time of a blob and lead to high erosion levels due to the non-linear dependence of the sputtering yield on the ion temperature. For more realistic SOL conditions with 1% impurity concentration, the blobs do not contribute significantly to the erosion anymore. The absolute erosion levels in this case, however, are substantial. The maximum gross erosion during a full year (365 d, 24 h/d) plasma operation of a hypothetical fusion reactor at ASDEX Upgrade L-mode conditions was estimated to be some millimeter on a tungsten PFC. Although this is an upper limit estimation since redeposition was not taken into account, it shows that the conditions in the SOL (high ion temperatures, filamentary convective transport, impurity concentration due to intended seeding or from first wall material) are highly relevant for an economic operation of a fusion power plant.

Acknowledgement

This project has received funding from the European Union's Horizon 2020 research and innovation programme under grant agreement number 633053. The views and opinions expressed herein do not necessarily reflect those of the European Commission. F. M. Laggner is a fellow of the Friedrich Schiedel Foundation for Energy Technology.

[1] H. Bolt *et al.*, Journal of Nuclear Materials **307-311**, (2002) 43-52
[2] T. Eich *et al.*, Plasma Phys. Control. Fusion **49**, 573-604 (2007)
[3] A. Herrmann, T. Eich, V. Rohde, C.J. Fuchs, J. Neuhauser and ASDEX Upgrade Team, Plasma Phys. Control. Fusion **46**, 971-979 (2004)
[4] H. Maier, and the ASDEX Upgrade Team, Journal of Nucl. Mat. **335**, 515-519 (2004)
[5] M. Kocan *et al.*, Plasma Phys. Control. Fusion **54**, 085009 (2012)
[6] D. A. D'Ippolito, J. R. Myra, and S. J. Zweben, Phys. Plasmas **18**, 060501 (2011)
[7] S. Krasheninnikov, Physics Letters A **283**, 368 (2001).
[8] D. Naujoks *et al.*, Nucl. Fus., Vol. 36, No. 6 (1996)
[9] M. Willensdorfer, E. Wolfrum, R. Fischer, J. Schweinzer, M. Sertoli, B. Sieglin, G. Veres, F. Aumayr, and the ASDEX Upgrade Team, Review of Scientific Instruments **83**, 023501 (2012).
[10] M. Willensdorfer *et al.*, Plasma Phys. Control. Fusion **56**, 025008 (2014)
[11] R. Fischer, E. Wolfrum, J. Schweinzer, and the ASDEX Upgrade Team, Plasma Physics and Controlled Fusion **50**, 085009 (2008).
[12] G. Birkenmeier *et al.*, Plasma Phys. Control. Fusion **56**, 075019 (2014)
[13] P. Manz *et al.*, Phys. Plasmas **20**, 102307 (2013)
[14] D. Carralero *et al.*, Nucl. Fusion **54**, 12300 (2014)
[15] M. Agostini *et al.*, Nucl. Fusion **51**, 053020 (2011)
[16] P.C. Stangeby, "The Plasma Boundary of Magnetic Fusion Devices",Institute of Physics Publishing, Bristol (2000)
[17] K. Schmid *et al.*, Nucl. Fusion **50**, 105004 (2010)
[18] A. Thoma *et al.*, Plasma Phys. Control. Fusion **39**, 1487-1499 (1997)
[19] R. Dux *et al.*, Journal of Nuclear Materials **390-391**, 858-863 (2009)
[20] G.F. Matthews and G.M. McCracken and P. Sewell and M. Woods and B.J. Hopkins, Journal of Nuclear Materials **145-147**, 225-230 (1987)
[21] M. Kocan *et al.*, Journal of Nuclear Materials **438**, S501-S504 (2013)
[22] J.P. Gunn, Plasma Phys. Controlled Fusion **54**, 085007 (2012)
[23] G.F. Matthews, R.A. Pitts, G.M. McCracken and P.C. Stangeby, Nucl. Fusion **31**, 1495 (1991)
[24] A. Herrmann *et al.*, Journal of Nuclear Materials **363-365**, 528-533 (2007)
[25] H.W. Müller and J. Adamek and R. Cavazzana and G.D. Conway and C. Fuchs and J.P. Gunn and A. Herrmann and J. Horacek and C. Ionita and A. Kallenbach and M. Kocan and M. Maraschek and C. Maszl and F. Mehlmann and B. Nold and M. Peterka and V. Rohde and J. Schweinzer and R. Schrittwieser and N. Vianello and E. Wolfrum and M. Zuin and the ASDEX Upgrade Team, Nucl. Fusion **51**, 073023 (2011)
[26] M. Shimada *et al.*, Nucl. Fusion **47**, S1 (2007)